A STUDY OF THE DYNAMICS OF HODOGRAPH ROTATION IN THE SEA BREEZES OF ATTICA, GREECE

D. G. STEYN

Atmospheric Science Programme, Department of Geography, The University of British Columbia, Vancouver, B.C. Canada, V 6T 1WS

and

G. KALLOS

Department of Applied Physics, University of Athens, Athens 10680, Greece

(Received 14 May, 1991)

Abstract. The diurnal evolution of the sea breeze hodograph over the Attic Peninsula has been studied using a three-dimensional numerical mesoscale model with fully nonlinear friction parameterization. The model results compare well with observed hodographs at three points in the modelling domain, and show that the balance of pressure gradient and terrain gradient forcing is dominant, and that this balance may result in either clockwise or anticlockwise rotation.

1. Introduction

The diurnal behaviour of sea breezes in the Saronic Gulf and the Attic peninsula (see Figure 1) were of importance in classical times when the Athenian General Themistocles, as reported in Plutarch's Parallel Lives (Themistocles, XIV. 2), took advantage of the morning onset and shoreward direction of the sea breeze (". . . until the hour had come which always brought the breeze fresh from the sea . . ." as translated by Perrin, 1914) in order to defeat the Persian fleet of King Xerxes in the Battle of Salamis (480 B.C.).

In modern times the same local wind system and the invariability of its diurnal behaviour are of importance because of their role in transporting photochemical pollutants in the Athens basin (Lalas *et al.*, 1983; Güsten *et al.*, 1988).

The Athens sea breeze has been subjected to considerable study using climatological methods (Zambakas, 1973; Carapiperis and Catsoulis, 1977; Prezerakos, 1986), observational methods (Lalas *et al.*, 1983; Asimakopoulos, 1985; Helmis *et al.*, 1987) and numerical modelling methods (Moussiopoulos, 1985; Moussiopoulos and Flassak, 1986; Kallos, 1987; Papageorgiou, 1988). These studies reveal a complicated horizontal flow-field whose diurnal evolution contains the reportedly (Zambakas, 1973 and Prezerakos, 1986) unusual (for the northern hemisphere) feature of backing (Anti-Clockwise Rotation, ACR) rather than the Coriolis-induced veering (Clockwise Rotation, CR) predicted by the linear sea breeze theory of Haurwitz (1947).

The spatial complexity of the wind field is presumed by Helmis *et al.* (1987), Lalas (1983), Prezerakos (1986) and Zambakas (1973) to be due to the complicated

Boundary-Layer Meteorology **58**: 215–228, 1992.

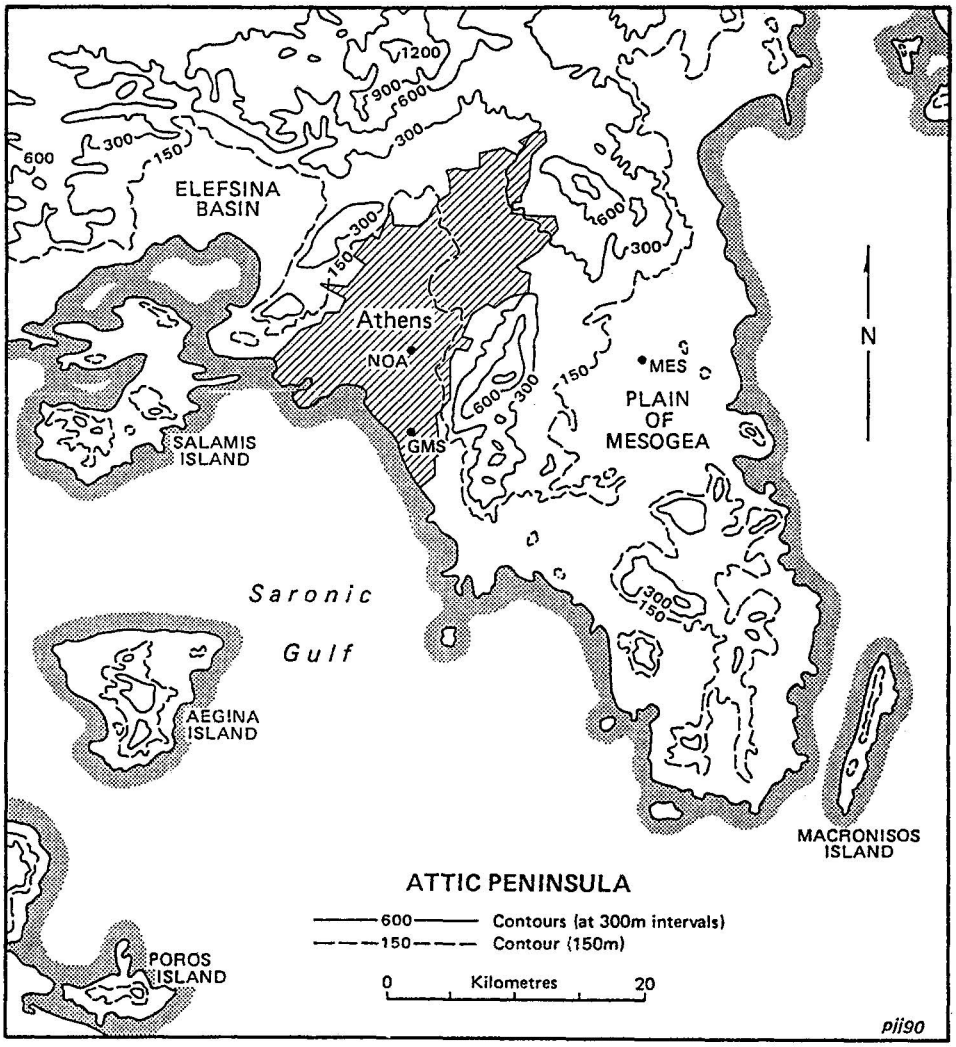

Fig. 1. Map of the modelling domain showing the coastline and terrain of the Attic Peninsula and the three observing stations (GMS, MES and NOA) referred to in the text.

coastline and topography of the Attic peninsula (Figure 1) while Asimakopoulos (1985) and Lalas (1983) point to the existence of sea breeze circulations in the neighbouring basin of Elefsina and the plain of Mesogea as contributing factors.

The diurnal evolution of the sea breeze at stations near the coast of the Saronic Gulf as a continuous ACR from 0900 to 2000 (local time) is revealed by the climatological hodographs of Zambakas (1973) and in the figures of Prezerakos (1986); the evolution is clearly evident in the observations of Lalas (1983) and is implicit in the sequence of modelled wind fields for one day generated by Kallos (1987). Prezerakos (1986) shows that the sea breeze at inland stations undergoes CR, and explains the coastal CR as being due to a regional circulation dominating

the Coriolis effect while Zambakas (1973) argues that the presence of the Saronic Gulf induces a southerly component which conceals the Coriolis effect.

Prezerakos (1986) and Zambakas (1973) appear to treat the ACR as an unusual feature while Kusuda and Alpert (1983) cite a number of observational studies of northern hemisphere sea breezes that exhibit ACR, thus showing that rotation in this sense is not completely unusual. Neumann (1577), Burk and Staley (1979) and Kusuda and Alpert (1983) provide a theoretical framework for the study of hodograph rotation, and show that the sense of rotation is controlled by the balance of forces (mesoscale pressure gradient, horizontal advection, vertical advection and friction) in the horizontal momentum equation. Kusuda and Alpert (1983) conclude that ACR is only possible in the presence of complex topography near the coastline.

The objective of this study is to perform a dynamical analysis similar to that of Burk and Staley (1979) and Kusuda and Alpert (1983) in order to explain the presence of both CR and ACR at a number of points within the sea breeze in the Attic peninsula. The climatological studies of Zambakas (1973), Carapiperis and Catsoulis (1977) and Prezerakos (1986) have pointed to the almost invariable pattern of evolution of the sea breeze from day to day, thus allowing general conclusions to be drawn from the examination of the evolution on a single day. For this study, we examine the dynamics of the sea breeze on 1981.08.12 studied by Kallos (1987). The study will rely on his 24-h simulation of the sea breeze on that day, using a three-dimensional mesoscale numerical model; the dynamical analysis will be based on an analysis of the forces as represented in the model. Following Zambakas (1973), we restrict ourselves to consideration of the hours 0900 to 2000 and thus concentrate on the sea breeze phase of the land/sea breeze cycle.

2. The Model, Modelling Domain and Input Data

The model employed in this study is a version of the mesoscale numerical model described by Pielke (1974), Pielke and Mahrer (1975, 1978) and Mahrer and Pielke (1977, 1978). The model was designed to study thermally-forced, terrain-induced mesoscale phenomena, is ideally suited to the study of sea breezes and has frequently been used for this purpose (Pielke, 1974; Kallos, 1987; Steyn and McKendry, 1988 for example). The model is hydrostatic, and consists of the equations of motion, moisture and continuity within a three-dimensional terrain-following coordinate system. It includes a thermodynamic equation, a diagnostic equation for pressure, a surface heat budget and a boundary-layer parameterization after Deardorff (1974). This parameterization includes a formulation for surface friction based on a stability-dependent vertical eddy exchange coefficient after Pielke and Mahrer (1975). Horizontal diffusion is not treated explicitly in the model, but is represented by a highly selective horizontal filter.

The modelling domain consists of a 26×28 horizontal grid with a 4 km grid

TABLE I

Initial input and boundary conditions for sea-breeze simulation on 1981.08.12 over the Attic Peninsula

Geostrophic wind speed	5.0 m/s
Geostrophic wind direction	330 deg
Atmospheric pressure at sea level	1008 hPa
Sea-surface temperature	299 K
Potential temperature lapse rate of free atmosphere	4 K/km
Initial PBL height	300 m
Roughness length over land	0.20 m
Specific humidity near surface	0.014
Surface albedo	0.2
Thermal conductivity of soil	0.0034 cal/(cm K s)
Soil density	1.45 g/cm^3
Thermal capacity of soil	0.31 cal/(g K s)
Soil wetness	0.05
Latitude	38° N
Upper absorbing layer	5.0–7.3 km
Time step	30 s
Initialization time	0500 local time

spacing in the inner 20 × 18 points and an expanding grid in the outer points. The model utilizes 19 vertical levels, closely spaced near the surface with the lowest level at 10 m above the surface. The terrain and coastlines of the inner grid of the modelling domain are shown in Figure 1. The outer grid also covered parts of the northeast Peloponnese and the island of Evia, both of which have been shown by Kallos (1987) to be important if the wind fields in the western Saronic Gulf are to be accurately represented. This terrain was averaged upward to a 4 km resolution from a 500 m digital terrain model and smoothed to remove 2 grid-length variations.

The initial and synoptic conditions prevailing on this day are summarised in Table I extracted from Kallos (1987). The synoptic conditions during the day studied were characterised by a thermal low pressure centre over Asia Minor and the Near East and a broad region of high pressure over Central and Eastern Europe, extending towards the central Mediterranean Sea. This latter high pressure region was in the process of decaying during the period under study. The resultant synoptic pressure gradient was less than 1 hPa per 100 km, producing a wind of approximately 5 m/s from the northnorthwest. Skies over the domain were generally clear, leading to strong insolation. This synoptic pattern is one which favours local, thermally-driven circulations, rather than the seasonal *Etesians* (Maheras, 1980).

3. Observed and Modelled Hodograph Rotation

It must first be established that the numerical model is able to reproduce the observed hodograph rotation. In order to do this, the modelled hodographs are compared with observed ones. The observations utilized are from three of the

stations in the Attic Peninsula used in the study by Lalas *et al.* (1983), which covers the day being modelled.

The stations for this study are chosen so as to use only data from well-exposed anemometers, and to illustrate both CR and ACR during the sea breeze. To this end, the stations labelled GMS (Greek Meteorological Service), NOA (National Observatory of Athens) and MES (Mesogea) are chosen (see Figure 1 for station locations). The station labelled NOA is the one used by Zambakas (1973), while that labelled GMS is the reference station of Prezerakos (1986). The observed data are all 10-min averages of wind speed and direction centered on each hour from 0900 to 2000, while the modelled wind speeds and directions are effectively 1-min averages valid for the hour given. While the model results are for points at the centers of the computational grid squares, the observing stations are generally not located at these centers. Since the distances from the observing stations to the grid centers is generally not large, and the modelled fields are relatively slowly varying in space, the modelled fields are not interpolated to the observation points. Hodographs showing observed and modelled winds at the three stations are presented in Figures 2a–2c.

Figures 2a and 2b show the diurnal evolution of the sea breeze at the stations NOA and GMS, respectively. In both cases, both modelled and observed winds show the ACR referred to by Zambakas (1973) and Prezerakos (1985). In the case of NOA, the winds are confined to the S to SSE sector by the topography of the basin in which the city of Athens is located. The hodograph at GMS shows winds from a much wider (but still largely onshore) sector in keeping with the station's location on the open coastal plain close to the shoreline. In both of these locations the model shows a tendency to overestimate the strength of the sea breeze while closely mimicking the observed directional evolution. This property of the model was noted by Steyn and McKendry (1986), who modelled sea-breezes in the similarly topographically constrained Fraser Valley of British Columbia. As may be expected, the observed wind exhibits a more complex temporal behaviour than the modelled wind. This is presumably due to local surface features which are unresolved by the modelling grid.

Figure 2c shows the diurnal evolution of the sea breeze at the station MES, where both modelled and observed winds exhibit CR. In this case (as in the previous two), the model matches the observed diurnal evolution of wind direction fairly well, but significantly overestimates the wind speed. Again, the modelled wind has much smoother behaviour than the observed. This station is located on the Eastern side of the Attic Peninsula, and experiences an entirely different sea breeze regime than the stations GMS and NOA, one of the major differences being the sense of hodograph rotation.

This brief analysis of modelled and observed hodographs at three stations within the modelling domain has shown that modelled and observed hodographs exhibit the same sense and rate of rotation, for stations having both CR and ACR. Based on this conclusion we assume that the balance of forces governing the diurnal

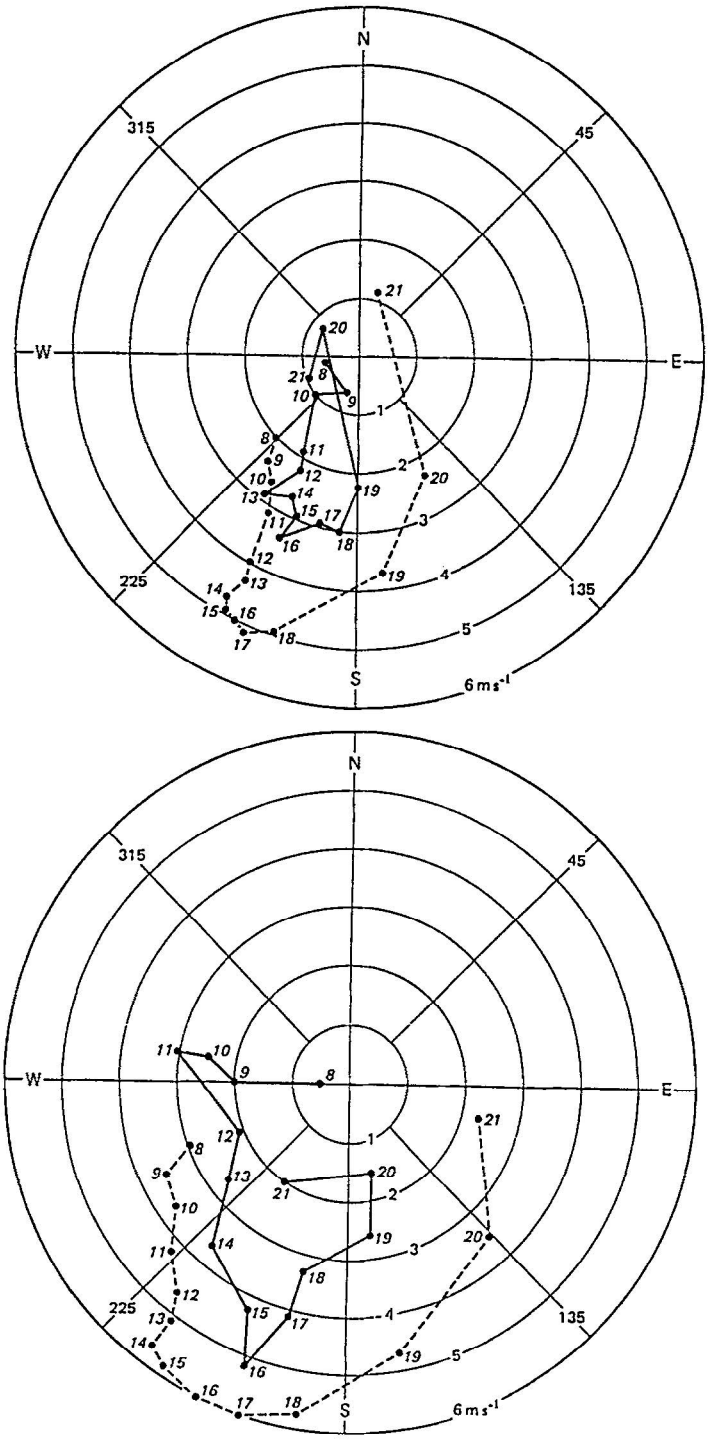

Fig. 2a and b.

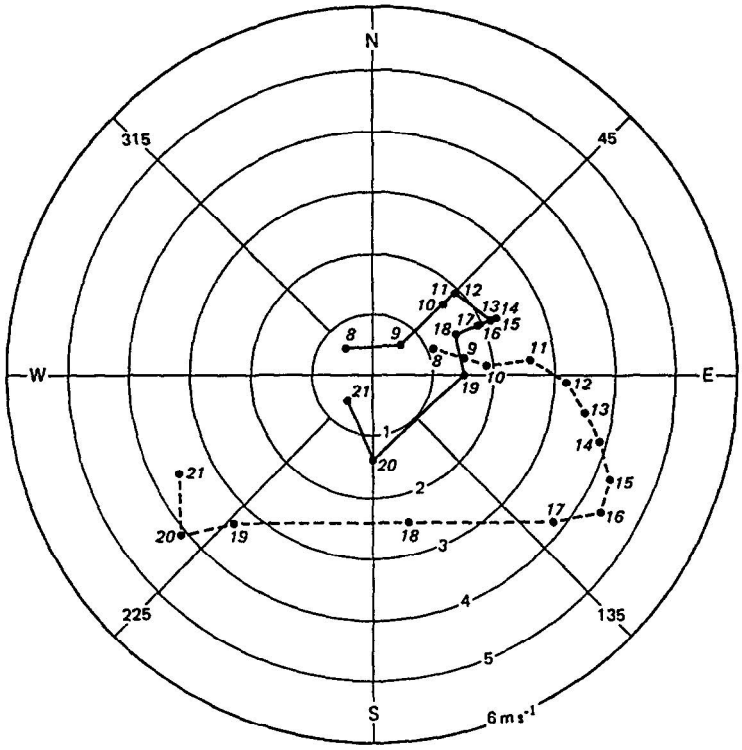

Fig. 2. Diurnal hodographs of observed (solid line) and modelled (broken line) winds at: (a) The National Observatory of Athens, (b) Greek Meteorological Service and (c) Mesogea.

evolution of the sea-breeze in the model will be a fair reflection of the actual balance of forces.

4. Imbalance of Forces Resulting in Hodograph Rotation

4.1. Wind direction tendency terms from a numerical model

The continual (on a daily time scale) evolution of the sea breeze is a result of the imbalance of the forces in a horizontal plane acting in the lower layers of the atmosphere. These forces are represented in the horizontal equation of motion by Mahrer and Pielke (1977) as:

$$\frac{du}{dt} = fv - fv_g - u\frac{\partial u}{\partial x} - v\frac{\partial u}{\partial y} - w^*\frac{\partial u}{\partial z^*} - \theta\frac{\partial \pi}{\partial x} + g\frac{z^* - \bar{s}}{\bar{s}}\frac{\partial z_G}{\partial x} - g\frac{z^*}{\bar{s}}\frac{\partial s}{\partial x} + \left(\frac{\bar{s}}{s - z_G}\right)^2 \frac{\partial}{\partial z^*}\left(K_z\frac{\partial u}{\partial z^*}\right) \quad (1)$$

$$\frac{dv}{dt} = -fu + fu_g - u\frac{\partial v}{\partial x} - v\frac{\partial v}{\partial y} - w^*\frac{\partial v}{\partial z^*}$$
$$- \theta\frac{\partial \pi}{\partial y} + g\frac{z^* - \bar{s}}{\bar{s}}\frac{\partial z_G}{\partial y} - g\frac{z^*}{\bar{s}}\frac{\partial s}{\partial y} \qquad (2)$$
$$+ \left(\frac{\bar{s}}{s - z_G}\right)^2 \frac{\partial}{\partial z^*}\left(K_z\frac{\partial v}{\partial z^*}\right)$$

where u and v are east-west and north-south components of the horizontal wind velocity, respectively, u_g and v_g are the east-west and north-south components of the (horizontal) geostrophic wind velocity, respectively, θ is the potential temperature, $\pi = c_p(P/P_{00})^{R/c_p}$ is Exner's function, c_p is the specific heat of air at constant pressure, P is pressure, P_{00} is a reference pressure, R is the gas constant for dry air, g is the acceleration due to gravity, $z^* = \bar{s}(z - z_G)/(s - z_G)$ is the vertical terrain-following coordinate, z_G is the terrain elevation, x and y are the east-west and north-south horizontal coordinates, respectively, s is the material surface at the top of the model, $\bar{s}$ is the initial value of s, and K_z is the vertical exchange coefficient of momentum; w^* is the vertical advection velocity defined by Mahrer and Pielke (1977) as:

$$w^* = \left(\frac{\bar{s}}{s - z_G}\right)w + \frac{z^*}{s - z_G}\left(\frac{\partial s}{\partial t} + u\frac{\partial s}{\partial x} + v\frac{\partial s}{\partial y}\right)$$
$$+ \frac{z^* - \bar{s}}{s - z_G}\left(u\frac{\partial z_G}{\partial x} + v\frac{\partial z_G}{\partial y}\right).$$

Following Kusuda and Alpert (1983), the rate of rotation of the horizontal wind vector $\mathbf{V}_H$ (with components u and v and magnitude $\mathbf{V}_H$) is:

$$\frac{\partial \alpha}{\partial t} = \frac{\mathbf{k}}{V_H^2}\left[\mathbf{V}_H \times \frac{\partial \mathbf{V}_H}{\partial t}\right], \qquad (3)$$

where α is the angle between the wind vector and the positive direction of the x-axis. Expanding the vector triple product in Equation (3), using the components of the horizontal wind velocity tendency in Equations (1) and (2), gives:

$$\frac{\partial \alpha}{\partial t} = \frac{f}{V_H^2}(\mathbf{V}_H \cdot \mathbf{V}_g - V_H^2) \qquad \text{Geostrophic departure}$$
$$+ \frac{\theta}{V_H^2}\left(v\frac{\partial \pi}{\partial x} - u\frac{\partial \pi}{\partial y}\right) \qquad \text{Pressure gradient}$$
$$+ \frac{g}{V_H^2}\frac{z^* - \bar{s}}{\bar{s}}\left(u\frac{\partial z_G}{\partial y} - v\frac{\partial z_G}{\partial x}\right) \qquad \text{Topographic gradient}$$
$$+ \frac{f}{V_H^2}\frac{z^*}{\bar{s}}\left(v\frac{\partial s}{\partial x} - u\frac{\partial s}{\partial y}\right) \qquad \text{Material surface gradient}$$

$$+\frac{1}{V_H^2}\frac{\bar{s}}{s-z_G}\left(u\frac{\partial}{\partial z^*}K_z\frac{\partial v}{\partial z^*}-v\frac{\partial}{\partial z^*}K_z\frac{\partial u}{\partial z^*}\right) \quad \text{Friction}$$

$$+\frac{1}{V_H^2}\left[uv\left(\frac{\partial u}{\partial x}-\frac{\partial v}{\partial y}\right)+v^2\frac{\partial u}{\partial y}-u^2\frac{\partial v}{\partial x}\right] \quad \text{Horizontal advection}$$

$$+\frac{1}{V_H^2}\left(vw^*\frac{\partial u}{\partial z^*}-vw^*\frac{\partial u}{\partial z^*}\right). \quad \text{Vertical advection} \qquad (4)$$

TABLE II

Terms in Equation (4) (scaled by f) for station GMS on 1981.08.03. The terms on the right hand side of the equation are: Geostrophic Departure (G.D.), Pressure Gradient (P.G.), Terrain Gradient (T.G.), Material Surface (M.S.), Friction (F.), Horizontal Advection (H.A.) and Vertical Advection (V.A.)

Time	$\partial\alpha/\partial t$	= G.D.	+ P.G.	+ T.G.	+ M.S.	+ F.	+ H.A.	+ V.A.
8	7.50	−0.76	112.5	−101.4	0.00	−6.49	3.67	0.00
9	5.88	−0.94	75.6	−64.2	0.00	−8.01	3.50	0.00
10	5.36	−1.14	45.7	−32.6	0.00	−10.59	4.02	−0.02
11	2.53	−1.28	15.6	−3.5	0.00	−12.71	4.47	−0.03
12	1.86	−1.38	−6.8	17.3	0.00	−11.84	4.63	−0.04
13	2.65	−1.37	−10.5	19.1	0.00	−9.21	4.69	−0.03
14	2.03	−1.35	−12.4	19.1	0.00	−8.09	4.83	−0.02
15	3.67	−1.39	−21.5	27.6	0.00	−5.68	4.59	−0.01
16	6.44	−1.47	−37.8	43.5	0.00	−2.16	4.33	0.00
17	7.58	−1.56	−52.9	58.7	0.00	−0.23	3.59	0.01
18	7.19	−1.67	−71.9	79.2	0.00	−0.08	1.62	0.00
19	6.72	−2.01	−127.4	137.2	0.00	−0.29	−0.79	0.01
20	6.98	−2.36	−209.0	216.0	0.00	−0.98	3.26	0.00
21	0.15	−2.50	−283.1	296.1	0.00	−1.38	1.06	0.02

The forcing term labelled "Material Surface Gradient" arises from the upper boundary of the model which is a flexible material surface whose slope can induce motion (mainly near the top of the model domain). The seven terms contributing to the rotation rate in Equation (4) are represented in finite difference form in the model, and their component variables are available as model output at each grid point within the domain for each hour. For the purposes of this dynamical analysis, the model variables at the lowest model level at the four grid points surrounding each of the observation stations are used to estimate the seven terms in Equation (4) using a simple centered finite-difference representation. For the friction term, values of the velocities and exchange coefficients at the lowest two levels and the two intermediate computational levels (Pielke, 1974) are needed. The values of the terms in Equation (4) for each of the three stations throughout the period 0900 to 2000 are given in Tables II–IV, where they are scaled by f.

4.2. Relative magnitudes of tendency terms

Table II shows that at the station GMS, the M.S. and V.A. terms are negligibly small as would be expected for a station near the coastline. The H.A. term induces

TABLE III

Terms in Equation (4) (scaled by f) for station NOA on 1981.08.03. The terms on the right hand side of the equation are: Geostrophic Departure (G.D.), Pressure Gradient (P.G.), Terrain Gradient (T.G.), Material Surface (M.S.), Friction (F.), Horizontal Advection (H.A.) and Vertical Advection (V.A.)

Time	$\partial\alpha/\partial t$	= G.D.	+ P.G.	+ T.G.	+ M.S.	+ F.	+ H.A.	+ V.A.
8	4.26	−1.60	−262.4	272.9	4.60	−8.44	−0.80	−0.02
9	4.42	−1.66	−265.9	277.1	4.30	−8.63	−0.80	−0.02
10	4.12	−1.81	−297.2	309.1	3.45	−8.76	−0.66	−0.02
11	3.64	−1.79	−276.6	287.5	2.64	−7.18	−0.95	0.00
12	3.40	−1.66	−229.1	237.8	2.40	−5.37	−0.65	0.00
13	2.95	−1.62	−216.8	223.9	2.23	−4.34	−0.44	0.00
14	2.74	−1.56	−195.9	201.5	1.97	−3.07	−0.18	0.00
15	3.10	−1.55	−192.5	197.5	2.06	−2.55	0.11	0.01
16	2.35	−1.57	−197.7	202.4	1.06	−2.22	0.35	0.01
17	1.69	−1.59	−200.3	204.3	0.11	−1.42	0.59	0.01
18	0.64	−1.69	−230.4	232.2	−0.79	0.06	1.18	0.01
19	0.83	−2.22	−381.0	382.2	−0.38	−0.20	2.39	0.00
20	−3.31	−3.11	−621.1	619.7	−0.28	−0.45	1.78	0.18
21	28.51	2.09	1063.7	−1038.4	−1.72	−1.24	2.94	1.10

TABLE IV

Terms in Equation (4) (scaled by f) for station MES on 1981.08.03. The terms on the right hand side of the equation are: Geostrophic Departure (G.D.), Pressure Gradient (P.G.), Terrain Gradient (T.G.) Material Surface (M.S.), Friction (F.), Horizontal Advection (H.A.) and Vertical Advection (V.A.)

Time	$\partial\alpha/\partial t$	= G.D.	+ P.G.	+ T.G.	+ M.S.	+ F.	+ H.A.	+ V.A.
8	21.49	−1.73	−704.7	714.4	7.58	5.93	−0.04	0.00
9	4.10	−2.19	−373.8	379.1	2.09	−2.43	1.35	0.00
10	−1.28	−2.15	−268.2	272.0	1.02	−6.29	2.32	0.00
11	−5.01	−1.84	−191.9	194.1	0.39	−8.83	3.12	0.00
12	−7.06	−1.87	−116.1	118.1	0.17	−11.24	3.81	0.00
13	−6.75	−1.93	−62.4	65.2	0.10	−11.41	3.66	0.00
14	−5.18	−1.95	−27.3	30.8	1.35	−11.53	3.42	0.00
15	−6.29	−1.97	10.1	−6.2	0.94	−11.68	2.56	0.00
16	−5.60	−2.01	40.5	−36.1	1.97	−12.12	2.15	0.00
17	−4.37	−2.22	83.4	−78.6	3.68	−11.73	1.16	0.00
18	−1-94	−2.91	335.3	−336.3	8.62	−0.45	−6.21	0.02
19	−4.07	−1.42	289.8	−296.2	1.10	0.21	2.42	−0.02
20	−3.82	−1.22	225.1	−228.8	−2.23	0.25	3.07	−0.02
21	−8.36	−0.95	224.9	−228.0	−6.50	−0.06	2.19	0.03

a roughly constant ACR, while the F. term induces a CR of variable strength, with the largest magnitude in the morning when the boundary layer is shallowest. The P.G. and T.G. terms have opposite senses, and are the largest of all the terms, while the F. term is generally somewhat larger than the remaining ones. The larger of the two dominant terms (P.G. and T.G.) is always the one inducing ACR. While all terms contribute to the total rotation, it may be said that the rotation sense at GMS is determined by a balance between the pressure gradient

and terrain gradient terms that are able to overcome the coriolis effect which is contained in the geostrophic departure term.

An inspection of Table III reveals that at NOA, as at GMS, the P.G. and T.G. terms are the largest ones, and have opposite signs, while the F. term is of secondary importance but generally larger than the remaining terms. In this case however, P.G. and T.G. induce consistently CR and ACR, respectively, with T.G. being the largest. The resultant rotation is ACR in response to the dominance of the terrain gradient term.

Table IV shows that the rotation at MES is again dominated by a balance between the P.G. and T.G. terms. In this case (as at GMS), the dominant terms have opposite signs, and the larger one is consistently the one inducing CR, which simply enhances the effect of the small but not insignificant geostrophic departure term. In this case, as in the previous ones, the influence of the F. term is secondary, but still greater than that of the G.D., M.S., H.A. and V.A. terms.

The analysis of the three cases has shown that while the V.A. term is generally not important in inducing hodograph rotation, all other terms play a role. The details of the resultant rotation can depend on the balance of the remaining terms in a quite complex way but, in the cases examined, depend largely on the balance of the P.G. and T.G. terms, which are in general much larger than the other terms and have opposite signs. This balance can result in either CR or ACR in different parts of the domain studied.

Kusuda and Alpert (1983) used a much simpler model to investigate CR and ACR regimes in a two-dimensional domain with artificial topography. Their model included a mesoscale pressure gradient term (equivalent to the sum or our P.G. and T.G. terms) which, in their analysis was the dominant term in inducing rotation, with the friction and Coriolis terms being ranked second and third, respectively. The conclusions of our analysis are substantially in agreement with those of Kusuda and Alpert (1983).

5. Regional Patterns of Hodograph Rotation

The model-simulated evolution of the sea breeze used to generate Tables II, III and IV can also be used to generate maps of hodograph rotation similar to those derived by Kusuda and Abe (1989) from observations. From the model-output winds at each hour, we can calculate the average rotation rate for each hourly interval. The contours of rotation rate are in general fairly complex maps, but a cursory examination reveals the existence of an invariant and fixed tongue of CR in a broad region of ACR. Figure 3 shows the position of this feature between the hours 0900 and 1600 local time by representing the zone occupied by the ACR/CR boundary as a stippled swath. The tongue of CR is linked to the topography of the Attic Peninsula so that the southwestern shore including the observation stations GMS and NOA) is in a region of ACR and the northeastern shore (including the observing station MES) is in the tongue of CR. The time-

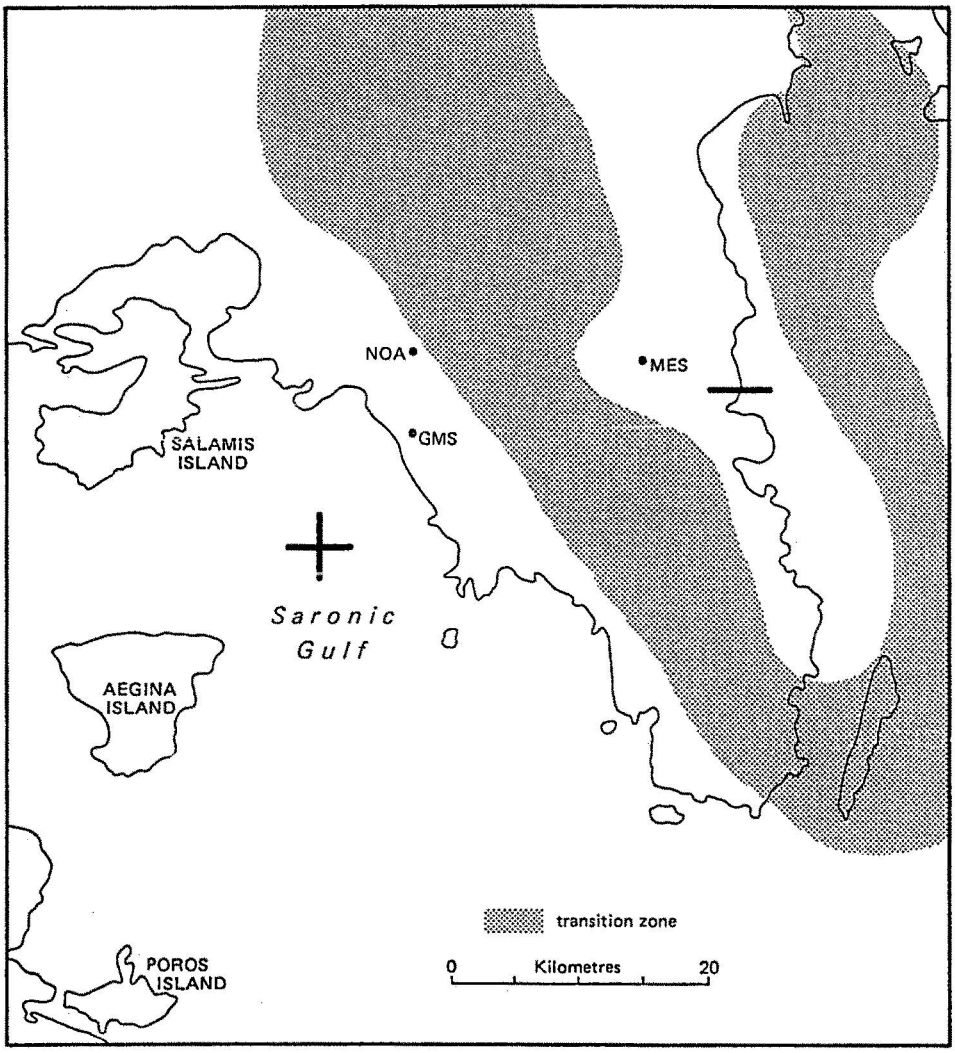

Fig. 3. Map showing the coastline of the Attic Peninsula and the regions of Anti-Clockwise Rotation (ACR) and Clockwise Rotation (CR) between the hours 0900 and 1600 local time. the stippled boundary between regions of ACR and CR indicates the position occupied by the individual (often quite convoluted) hourly boundaries between ACR and CR.

invariant position of the ACR/CR boundary is another representation of the invariant behaviour of the sea breeze over the Attic Peninsula.

6. Conclusions

The diurnal evolution of the sea breeze hodograph over the Attic Peninsula has been studied using a three-dimensional numerical mesoscale model with fully nonlinear friction parameterization. The model results compare well with observed

hodographs at three points in the modelling domain, and show that the balance of pressure-gradient and terrain-gradient forcing is dominant, and that this balance may result in either CR or ACR. It is shown that a broad region of CR is associated with the topography of the Attic Peninsula. Earlier speculations about the cause of the supposedly anomalous ACR in the Athens basin are shown to be mistaken.

Acknowledgements

This study was undertaken while DGS was on study leave supported in part by a UBC Izaac Walton Killam Memorial Faculty Research Fellowship. The work was partly funded by the General Secretariat of Research and Technology of Greece (contract 6845(ERE) 855/7-11-84 to GBK) and grants from the Natural Science and Engineering Research Council and the Atmospheric Environment Service of Canada to DGS. We are grateful to Ray Arritt and Xubin Zheng for advice on the derivation of the tendency terms from the model output files, and to Pinhas Alpert for comments on an early draft of this paper.

References

Asimakopoulos, D. N.: 1985, 'Final Report on Tidal Air Motions in the Athens Basin', *Contract Number B6612/9 Report for EEC/DGXI and Greek Ministry of the Environment*, 142 pp.

Burk, S. D. and Staley, D. O.: 1979, 'Comments "On the Rotation Rate of the Direction of Sea and Land Breezes"', *J. Atmos. Sci.* **36**, 369–371.

Carapiperis, L. N. and Catsoulis, V. D.: 1977, 'Contribution to the Study of Sea Breezes in Athens Area During Winter', *Bull. Hellenic Met. Soc.* **2**, 1–18 (in Greek).

Deardorff, J. W.: 1974, 'Three Dimensional Numerical Study of Height and Mean Structure of the Heated Planetary Boundary Layer', *Boundary-Layer Meteorol.* **7**, 81–106.

Güsten, H., Heinrich, G., Cvitaš, T., Klasinc, L., Ruš, B., Lalas, D. P., and Petrakis, M.: 1988, 'Photochemical Formation and Transport of Ozone in Athens, Greece', *Atmos. Env.* **22**, 1855–1861.

Haurwitz, B.: 1947, 'Comments on the Sea-Breeze Circulation', *J. Meteorol.* **4**, 1–8.

Helmis, C. G., Asimakopoulos, D. N., Deligiorgi, D. G., and Lalas, D. P.: 1987, 'Observations of Sea Breeze Fronts Near the Shoreline', *Boundary-Layer Meteorol.* **38**, 395–410.

Kallos, G.: 1987, 'A Simulation of the Atmospheric Circulations over Attica with a Three Dimensional Mesoscale Atmospheric Model: A Sea Breeze Case. Final Report Prepared for the General Secretariat of Research and Technology', *Contract 6845 (ERE) 855/7-11-84*, 159 pp. (in Greek).

Kusuda, M. and Abe, N.: 1989, 'The Contribution of Horizontal Advection to the Diurnal Variation of the Wind Direction of Land-Sea Breezes: Theory and Observations', *J. Meteorol. Soc. Japan* **67**, 177–184.

Kusuda, M. and Alpert, P.: 1983, 'Anticlockwise Rotation of the Wind Hodograph. Part I: Theoretical Study', *J. Atmos. Sci.* **40**, 487–499.

Lalas, D. P.: 1983, 'Analysis of Tidal Air Movements in Athens', *Technical Report. MPP-HE-EEC*, 43 pp.

Lalas, D. P., Asimakopoulos, D. N., Deligiorgi, D. G., and Helmin, C. G.: 1983, 'Sea Breeze Circulation and Photochemical Pollution in Athens, Greece', *Atmos. Env.* **17**, 1621–1632.

Maheras, P.: 1980, 'Le Problem des Etesiens', *Mediterranee* **4**, 57–66.

Mahrer, Y. and Pielke, R. A.: 1977, 'The Effects of Topography on Sea and Land Breezes in a Two Dimensional Numerical Model', *Mon. Wea. Rev.* **105**, 1151–1162.

Mahrer, Y. and Pielke, R. A.: 1978, 'A Test of an Upstream Spline Interpretation Technique for the Advection Terms in a Numerical Mesoscale Model', *Mon. Wea. Rev.* **106**, 818–830.

Moussiopolous, N.: 1985, 'A Numerical Simulation of the Sea Breeze in Athens', *Pageoph.* **123**, 314–327.

Moussiopolous, N. and Flassak, Th.: 1986, 'Two Vectorized Algorithms for the Effective Calculations of Mass-Consistent Flow Fields', *J. Clim. Appl. Meteorol.* **25**, 847–857.

Neumann, J.: 1977, 'On the Rotation Rate of the Direction of Sea and Land Breezes', *J. Atmos. Sci.* **34**, 1913–1917.

Pielke, R. A.: 1974, 'A Three Dimensional Numerical Model of the Sea Breezes over South Florida', *Mon. Wea. Rev.* **102**, 115–134.

Pielke, R. A. and Mahrer, Y.: 1975, 'Representation of the Heated Planetary Boundary Layer in Mesoscale Models with Course Vertical Resolution', *J. Atmos. Sci.* **32**, 2288–2308.

Pielke, R. A. and Mahrer, Y.: 1978, 'Verification Analysis of the University of Virginia Three-Dimensional Mesoscale Model Prediction over South Florida for 1 July 1973', *Mon. Wea. Rev.* **106**, 1568–1589.

Papageorgiou, J. G.: 1988, 'A 3-D Sea Breeze Model of the PBL Including Pollutant Dispersion', *Boundary-Layer Meteorol.* **45**, 9–30.

Pettin, B.: 1914, *Plutarch's Lives II.* Heinmann, London, 626.

Prezerakos, N. G.: 1986, 'Characteristics of the Sea Breeze in Attica, Greece', *Boundary-Layer Meteorol.* **32**, 245–266.

Steyn, D. G. and McKendry, I. G.: 1988, 'Quantitative and Qualitative Equalation of a Three-Dimensional Mesoscale Numerical Model Simulation of a Sea Breeze in Complex Terrain', *Mon. Wea. Rev.* **116**, 1914–1926.

Zambakas, J. D.: 1973, 'The Diurnal Variability and Duration of the Sea Breeze at the National Observatory of Athens, Greece', *Meteorol. Mag.* **102**, 222–228.